

Multiscaling in superfluid turbulence: A shell-model study

Vishwanath Shukla^{1,*} and Rahul Pandit^{2,†}

¹*Laboratoire de Physique Statistique de l'Ecole Normale Supérieure,
24 Rue Lhomond, 75231 Paris, France*

²*Centre for Condensed Matter Theory, Department of Physics,
Indian Institute of Science, Bangalore 560012, India.*

(Dated: September 29, 2018)

We examine the multiscaling behavior of the normal- and superfluid-velocity structure functions in three-dimensional superfluid turbulence by using a shell model for the three-dimensional (3D) Hall-Vinen-Bekharevich-Khalatnikov (HVBK) equations. Our 3D-HVBK shell model is based on the Gledzer-Okhitani-Yamada (GOY) shell model. We examine the dependence of the multiscaling exponents on the normal-fluid fraction and the mutual-friction coefficients. Our extensive study of the 3D-HVBK shell model shows that the multiscaling behavior of the velocity structure functions in superfluid turbulence is more complicated than it is in fluid turbulence.

PACS numbers: 67.25.dk, 47.37.+q, 67.25.dm, 67.25.D-

Keywords: superfluid; turbulence; multiscaling; mutual friction

I. INTRODUCTION

The characterization of energy spectra and velocity structure functions [1] occupies a central place in the elucidation of the statistical properties of turbulence, be it in fluids [1–8], conducting fluids [9–12], or superfluids [13–17]. For example, in fluid turbulence, we often use the longitudinal velocity \mathbf{v} structure function $S_p(r) \equiv \langle [\delta v(r)]^p \rangle$, where $\delta v(r) \equiv [\mathbf{v}(\mathbf{x} + \mathbf{r}) - \mathbf{v}(\mathbf{x})] \cdot [\mathbf{r}/r]$, which scales as $S_p(r) \sim r^{\zeta_p}$, for $r \equiv |\mathbf{r}|$ in the inertial range $\eta_d \ll r \ll L$; viscous dissipation is significant below the dissipation length scale η_d ; and L is the large length scale at which energy is injected into the fluid. The exponents ζ_p , which characterize multiscaling, are nonlinear, monotone increasing functions of p [1]; simple scaling is obtained if ζ_p depends linearly on p , as in the K41 phenomenological approach of Kolmogorov [18–20] that yields $\zeta_p^{K41} = p/3$.

Direct numerical simulations (DNSs) play an important role in studies of structure-function multiscaling in fluid turbulence [1, 5, 6]; such DNSs have achieved impressive spatial resolutions (see, e.g., Refs. [1, 5]). By contrast, DNS studies of superfluid turbulence, whether at the level of the Gross-Pitaevskii (GP) equation ([21, 22] and references therein) or via the Hall-Vinen-Bekharevich-Khalatnikov (HVBK) equations ([17, 23] and references therein), have only achieved modest spatial resolutions. Furthermore, the large number of parameters in these equations, e.g., the mutual-friction coefficients, the ratio of the normal-fluid density to the superfluid density, and the Reynolds number, pose a significant challenge for systematic studies of the multiscaling of normal-fluid- and superfluid-velocity structure func-

tions. It has been suggested, therefore, that shell models for the three-dimensional (3D) HVBK equations [24–26] be used first to study such multiscaling in detail.

Ever since their introduction in the early work of Obukhov [27], Desnyansky and Novikov [28], and Gledzer, and Okhitani and Yamada [29, 30] (henceforth GOY), shell models have played valuable roles in elucidating the multiscaling properties of structure functions of fluid turbulence [1, 31–38]. Over the years, such shell models have been used to study magnetohydrodynamic (MHD) turbulence [39–44], Hall-MHD turbulence [45–48], fluid turbulence with polymer additives [49], fluid turbulence in two dimensions [50], fluid turbulence in dimensions in between two and three [51], turbulence in binary-fluid mixtures [52] and in rotating systems [53], and, as we have mentioned above, turbulence in superfluids [24–26]. Shell models have also been used to initiate studies of the dynamic multiscaling of time-dependent structure functions [54–56].

We build on the shell-model studies of Refs. [24–26] to explore the dependence of the multiscaling exponents here on the parameters of the 3D HVBK model. It has been noted in Ref. [26] that, given current computational resources, a systematic study of this parameter dependence lies beyond the scope of a well-resolved DNS of the 3D HVBK equations; however, such a study is possible if we use shell models for these equations. Our study extends the work of Refs. [24–26] by obtaining a variety of results, which we summarize, before we present the details of our study.

Our study of the 3D-HVBK shell model shows that the multiscaling behavior of the shell-model counterparts of velocity structure functions in superfluid turbulence is more rich than that reported in Ref. [26]. Our results agree with those of Ref. [26] qualitatively insofar as we find that, in the limits when the normal-fluid fraction is either small (pure superfluid) or large, the equal-time multiscaling exponents are close to their classical-fluid-turbulence values. In addition, we find that there are

* research.vishwanath@gmail.com

† rahul@physics.iisc.ernet.in;

also at Jawaharlal Nehru Centre For Advanced Scientific Research, Jakkur, Bangalore, India.

two regions, with intermediate values of the normal-fluid fraction, in which the multiscaling exponents are larger than those observed for the classical-fluid-turbulence or even Kolmogorov's 1941 (K41) predictions [1]; between these two regions there is a region in which the multiscaling exponents are close to their K41 values. We have also investigated the dependence of the multiscaling exponents on the mutual-friction coefficient, with equal proportions of superfluid and normal-fluid components; here, our results show that, for small (weak-coupling limit) and large (strong-coupling limit) values of the mutual-friction coefficient, the multiscaling exponents tend to their classical-fluid-turbulence values, whereas, in an intermediate range, there are deviations from the classical-fluid-turbulence behavior; in particular, the multiscaling exponents are larger than their classical-fluid-turbulence counterparts for high-order structure functions (order $p \geq 3$).

The remainder of this paper is organized as follows. In Sec. II we describe the shell model and the numerical methods we use. Section III is devoted to our results. We end with conclusions in Sec. IV.

II. MODELS AND NUMERICAL SIMULATIONS

The GOY shell model, for the 3D Navier-Stokes equation [29, 30] for a fluid, comprises the following ordinary differential equations (ODEs):

$$\left[\frac{d}{dt} + \nu k_m^2 \right] u_m = \imath [ak_m u_{m+1} u_{m+2} + bk_{m-1} u_{m-1} u_{m+1} + ck_{m-2} u_{m-1} u_{m-2}]^* + f_m; \quad (1)$$

here we label shells by the positive integers m , in a logarithmically discretized Fourier space, with scalar wave numbers $k_m = k_0 \lambda^m$, where $k_0 = 2^{-4}$ and $\lambda = 2$. The $*$ denotes complex conjugation, ν is the kinematic viscosity, and $u_m(k_m)$ are the complex, scalar, shell velocities. The coefficients $a = 1$, $b = -\delta$, $c = -(1 - \delta)$ are chosen to conserve the shell-model analogs of energy and helicity in the limit of vanishing viscosity and the absence of external forcing; the standard value of δ is $1/2$; N is the total number of shells; and f_m is the external forcing, which is used to drive the system into a turbulent state that is statistically steady. The logarithmic discretization of Fourier space allows us to achieve very high Reynolds numbers, even with a moderate number of shells. In the GOY-shell-model equations, direct interactions are limited to the nearest- and next-nearest-neighbor shells; in contrast, if we write the Navier-Stokes equation in Fourier space, every Fourier mode of the velocity is directly coupled to every other Fourier mode.

The simplest form of the incompressible, 3D HVBK

equations [13, 57] is

$$\rho_s \frac{D\mathbf{u}^s}{Dt} = -\frac{\rho_s}{\rho} \nabla p + \rho_s \sigma \nabla T + \mathbf{F}_{mf}^s, \quad (2a)$$

$$\rho_n \frac{D\mathbf{u}^n}{Dt} = -\frac{\rho_n}{\rho} \nabla p - \rho_n \sigma \nabla T + \mathbf{F}_{mf}^n + \nu_n \nabla^2 \mathbf{u}^n, \quad (2b)$$

with $D\mathbf{u}^i/Dt = \partial \mathbf{u}^i / \partial t + \mathbf{u}^i \cdot \nabla \mathbf{u}^i$, the incompressibility condition $\nabla \cdot \mathbf{u}^i = 0$, and the superscript $i \in (n, s)$ denotes the normal fluid (n) or the superfluid (s); p , σ , and T are the pressure, specific entropy, and temperature, respectively; ρ_n (ρ_s) is the normal-fluid (superfluid) density; ν_n is the kinematic viscosity of the normal fluid. The mutual-friction terms, which model the interaction between the normal and superfluid components, can be written as $\mathbf{F}_{mf}^s = -(\rho_n/\rho) \mathbf{f}_{mf}$ and $\mathbf{F}_{mf}^n = (\rho_s/\rho) \mathbf{f}_{mf}$ in Eqs. (2a) and (2a), respectively, where

$$\mathbf{f}_{mf} = \frac{B}{2} \frac{\omega_s}{|\omega_s|} \times (\omega_s \times \mathbf{u}_{ns}) + \frac{B'}{2} \omega_s \times \mathbf{u}_{ns}, \quad (3)$$

with $\mathbf{u}_{ns} = (\mathbf{u}_n - \mathbf{u}_s)$ the slip velocity, and B and B' the coefficients of mutual friction. In most of our studies we set $B' = 0$, so $\mathbf{f}_{mf} = -\frac{B}{2} |\omega_s| \mathbf{u}_{ns}$, which is the Gorter-Mellink form [58].

We use the following shell model for the 3D HVBK equations; it is based on the GOY shell model for a fluid [24].

$$\left[\frac{d}{dt} + \nu_n k_m^2 \right] u_m^n = \text{NL}[u_m^n] + F_m^n + f_m^n, \quad (4)$$

$$\left[\frac{d}{dt} + \nu_s k_m^2 \right] u_m^s = \text{NL}[u_m^s] + F_m^s + f_m^s, \quad (5)$$

where

$$\text{NL}[u_m] = \imath [ak_m u_{m+1} u_{m+2} + bk_{m-1} u_{m-1} u_{m+1} + ck_{m-2} u_{m-1} u_{m-2}]^*. \quad (6)$$

Here, as in the GOY model, we have a logarithmically discretized Fourier space with shell- m wave numbers $k = k_0 \lambda^m$, where $k_0 = 2^{-4}$ and $\lambda = 2$, and kinematic viscosities ν_n and ν_s for the normal fluid and the superfluid, respectively; of course, ν_s must vanish in a superfluid but, in practical numerical simulations, $\nu_n \gg \nu_s > 0$ for numerical stability. The normal and superfluid dynamical variables are, respectively, the complex, scalar, shell velocities $u_m^n(k_m)$ and $u_m^s(k_m)$; and f_m^n and f_m^s are the external forcing terms. The coefficients $a = 1$, $b = -1/2$, $c = -1/2$ are chosen to conserve the shell-model analogs of energy and helicity in the limit of vanishing viscosity and the absence of external forcing. The shell-model analogs of the mutual-friction terms, which models the interaction between the normal and the superfluid components, are

$$F_m^s = \frac{\rho_n B \Omega_s^{1/2}}{2\rho} (u_m^n - u_m^s) \quad (7)$$

and

$$F_m^n = -\frac{\rho_s B \Omega_s^{1/2}}{2\rho} (u_m^n - u_m^s). \quad (8)$$

The shell-model superfluid and normal-fluid enstrophies are, respectively,

$$\Omega_s = \sum_{m=1}^N \frac{1}{2} k_m^2 |u_m^s|^2 \quad (9)$$

and

$$\Omega_n = \sum_{m=1}^N \frac{1}{2} k_m^2 |u_m^n|^2. \quad (10)$$

The total energy is

$$E_T = E_n + E_s \equiv \frac{1}{2} \sum_{m=1}^N (|u_m^n|^2 + |u_m^s|^2), \quad (11)$$

where E_n and E_s are the normal-fluid and superfluid energies, respectively. Other statistical quantities that we use in our study are as follows: The helicity is

$$H_i = \sum_{m=1}^N \frac{1}{2} \left(\frac{a}{c}\right)^m \frac{|u_m^i|^2}{k_m}; \quad (12)$$

the energy spectra are

$$E_i(k_m) = \frac{1}{2} \frac{|u_m^i|^2}{k_m}; \quad (13)$$

the root-mean-square velocities are

$$u_{\text{rms}}^i = \left(\sum_m |u_m^i|^2 \right)^{1/2}; \quad (14)$$

the Taylor microscale is

$$\lambda_i = \left[\frac{\sum_m E^i(k_m)}{\sum_m k_m^2 E^i(k_m)} \right]^{1/2}; \quad (15)$$

the Taylor-microscale Reynolds number is

$$Re_\lambda^i = u_{\text{rms}} \lambda_i / \nu_i; \quad (16)$$

the integral length scale is

$$\ell_I = \frac{\sum_m E^i(k_m) / k_m}{\sum_m E^i(k_m)}; \quad (17)$$

and the large-eddy-turnover time is

$$T_{\text{eddy}}^i = \frac{1}{k_1 u_1^i}; \quad (18)$$

here and henceforth $i \in (n, s)$.

The equal-time, order- p structure functions for the shell model are

$$S_p^i(k_m) \equiv \left\langle [u_m^i(t) u_m^{i*}(t)]^{p/2} \right\rangle \sim k_m^{-\zeta_p^i}, \quad (19)$$

where the power-law dependence is obtained only if k_m^{-1} lies in the inertial range. The structure functions defined above show period-three oscillations because of three cycles in the static solutions of the GOY model for the Navier-Stokes equation [33]. Therefore, we use the modified structure functions [32, 33]

$$\Sigma_p^i \equiv \left\langle \left| \Im [u_{m+2}^i u_{m+1}^i u_m^i - \frac{1}{4} u_{m-1}^i u_m^i u_{m+1}^i] \right|^{p/3} \right\rangle \sim k_m^{-\zeta_p^i}, \quad (20)$$

which filter out these oscillations effectively. The Sabra-model variant [25, 26] of the 3D HVBK equations does not show such oscillations. We expect that the multiscaling exponents ζ_p^i , $i \in (n, s)$, satisfy the following convexity inequality for any three positive integers $p_1 \leq p_2 \leq p_3$ [1]:

$$(p_3 - p_1) \zeta_{2p_2}^i \geq (p_3 - p_2) \zeta_{2p_1}^i + (p_2 - p_1) \zeta_{2p_3}^i. \quad (21)$$

We obtain smooth energy spectra, without period-3 oscillations, by using $E_i(k_m) = \Sigma_2^i(k_m) / k_m$, $i \in (n, s)$.

To obtain a turbulent, but statistically steady, state, we force both the superfluid and the normal-fluid components with the forces

$$f_m^{n,s} = (1 + \iota) \times 5 \times 10^{-3} \delta_{1,m}, \quad (22)$$

where $\delta_{1,m}$ is the Kronecker delta. We use the second-order, slaved Adams-Bashforth scheme to integrate the 3D-HVBK-shell-model Eqs. (4) and (5) [32, 59]. To study the multiscaling behaviors of structure functions here, we design the following three sets of runs:

1. **G1a-G9**: In these runs, we use the values of ρ_n/ρ and B , which have been measured at different temperatures in experiments on helium II [60]. We use suitable values of ν_n and ν_s , which we list, along with other parameters, in Table I.
2. **B1-B19**: We vary ρ_n/ρ between 0.05–0.95 and keep $B = 1.5$ fixed.
3. **R1-R12**: We vary B between 0.1–10 and keep $\rho_n/\rho = 0.5$ fixed.

In the runs B1-B19 and R1-R12, we use $\nu_n = 10^{-7}$, $\nu_s = 10^{-9}$, and the time step $\Delta t = 10^{-5}$.

We use the initial condition $u_m^{n,s} = (1 + \iota) k_m e^{-k_m^2}$, for $1 \leq m \leq N$, in the runs G1a-G9, PG1, and PG2; the GOY-shell-model runs PG1 ($\nu_n = 10^{-7}$) and PG2 ($\nu_n = 10^{-9}$) are included for the purpose of comparison with the runs G1a-G9. In the runs B1-B19 and R1-R12, we use the initial values $u_m^{n,s} = u_0^{n,s} k_m^{1/2} e^{-k_m^2} e^{i\vartheta_m}$, for $1 \leq m \leq N$, where ϑ_m is a random phase distributed uniformly on $[0, 2\pi)$. We use the boundary conditions $u_{-2}^i = u_{-1}^i = u_0^i = 0$ and $u_{N+1}^i = u_{N+2}^i = 0$, $i \in (n, s)$. We report results for $N = 36$ shells; Ref. [24] uses $N = 18$ and Ref. [26] presents data with $N = 36$.

	ρ_n/ρ	B	ν_n	ν_s	Δt
PG1	—	—	10^{-7}	—	10^{-5}
PG2	—	—	10^{-9}	—	10^{-5}
G1a	0.0450	1.5260	10^{-7}	10^{-10}	5.0×10^{-6}
G1	0.0450	1.5260	10^{-7}	10^{-9}	10^{-5}
G2	0.0998	1.3255	10^{-7}	10^{-9}	10^{-5}
G3	0.2503	1.0765	10^{-7}	10^{-9}	10^{-5}
G4	0.4004	0.9838	10^{-7}	10^{-9}	10^{-5}
G5	0.4994	0.9848	10^{-7}	10^{-9}	10^{-5}
G6	0.6003	1.0447	10^{-7}	10^{-9}	10^{-5}
G7	0.6493	1.1034	10^{-7}	10^{-9}	10^{-5}
G8	0.6995	1.1924	10^{-7}	10^{-9}	10^{-5}
G9	0.7501	1.3267	10^{-7}	10^{-9}	10^{-5}

TABLE I. Parameters for our 3D-shell-model runs (classical-fluid-turbulence) PG1, PG2 and 3D-HVBK-shell-model runs G1a-G9: ρ_n/ρ is the normal-fluid density fraction; B is the mutual-friction coefficient; ν_n (ν_s) is the normal-fluid (superfluid) viscosity; Δt is the time step; we use $N = 36$ shells in our simulations.

III. RESULTS

We now present the results of our study of superfluid and normal-fluid turbulence in the 3D-HVBK shell-model. We begin with energy spectra and then examine the parameter dependence of the exponents that characterize the multiscaling of structure functions.

In Table II we list the values of λ_i , Re_λ^i , and T_{eddy}^i that we obtain from our 3D-HVBK-shell-model simulations PG1, PG2, and G1a-G9. Figure 1 compares $E_n(k_m)$ (full curves) and $E_s(k_m)$ (dashed curves) for four representative values of ρ_n/ρ (runs G1 (purple curves), G2 (green curves), G5 (sky-blue curves), and G9 (brown curves)). The inertial ranges of $E_n(k_m)$ and $E_s(k_m)$ exhibit scaling that is consistent with a $k^{-5/3}$ power-law form (orange, dashed line); of course, this exponent is not exactly $-5/3$ if the structure functions display multiscaling. The runs PG1 and PG2 can be regarded as uncoupled ($B = 0$) normal fluid and superfluid, respectively; we use them for the sake of comparison with other runs to show how the mutual friction modifies the energy spectra. When we couple the normal and superfluid components, as in the run G1, $E_n(k_m)$ is pulled up towards $E_s(k_m)$, by virtue of the mutual-friction-induced tendency of locking between u_n and u_s (see Ref. [17]); in contrast, in the absence of coupling, the spectra $E(k_m)$ for the runs PG1 (yellow, full curves) and PG2 (yellow, dashed curves) lie far apart, especially in the dissipation range.

We study the multiscaling behaviors of the velocity structure functions for the 3D-HVBK shell-model by calculating the multiscaling exponents ζ_p^n and ζ_p^s , for the normal fluid and superfluid components, respectively, by using the Eqs. (20) for Σ_p^i . In Table III in the Supplemental Material, we list the values of these exponents, which

	λ_n	λ_s	$Re_\lambda^n (\times 10^6)$	$Re_\lambda^s (\times 10^8)$	T_{eddy}^n	T_{eddy}^s
PG1	0.95	—	7.2	—	14.50	—
PG2	0.50	—	310	—	20.33	—
G1a	0.42	0.28	2.3	15	45.61	45.61
G1	0.70	0.51	4.2	3.1	21.80	21.80
G2	0.73	0.54	4.4	3.2	22.03	22.03
G3	0.82	0.61	5.2	3.9	19.83	19.83
G4	0.71	0.54	4.4	3.4	18.41	18.41
G5	0.89	0.70	6.2	4.9	17.15	17.15
G6	0.94	0.77	6.9	5.6	15.45	15.45
G7	0.94	0.78	7.0	5.9	14.94	14.94
G8	0.95	0.80	7.2	6.1	14.51	14.51
G9	0.95	0.82	7.3	6.3	14.42	14.42

TABLE II. Parameters from our shell-model runs PG1, PG2, and G1a-G9: λ_n (λ_s) is the Taylor microscale for the normal-fluid (superfluid); Re_λ^n (Re_λ^s) is the Taylor-microscale Reynolds number for the normal-fluid (superfluid); T_{eddy}^n (T_{eddy}^s) is the large-eddy-turnover time for the normal-fluid (superfluid).

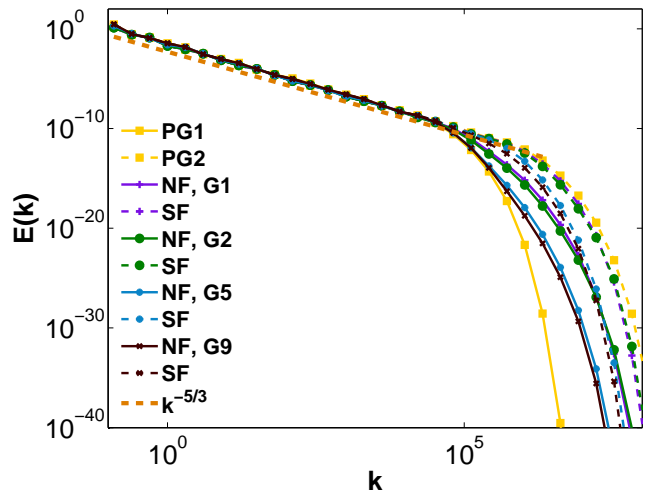


FIG. 1. Log-log (base 10) plots of the spectra $E_n(k_m)$ (full curves) and $E_s(k_m)$ (dashed curves) from our shell-model runs: PG1 and PG2 (yellow curves); G1 (purple curves); G2 (green curves); G5 (sky-blue curves); G9 (brown curves); a $k^{-5/3}$ power law is shown by the orange-dashed line; NF (SF) stands for normal-fluid (superfluid).

we have obtained from Σ_p^i , for $p = 1$ to 6, $i \in (n, s)$; each row of this Table has two lines; the first and second lines contain, respectively, the values of ζ_p^n and ζ_p^s . Table III (Supplemental Material) shows that $\zeta_p^n = \zeta_p^s$, for $p = 1$ to 6, for the runs G1-G9, because of the mutual-friction-induced locking of the normal fluid and superfluid velocities in the inertial range.

Figures 2 (a) and (b) show, respectively, plots of ζ_p^n and ζ_p^s versus the order p ; in these plots the orange line

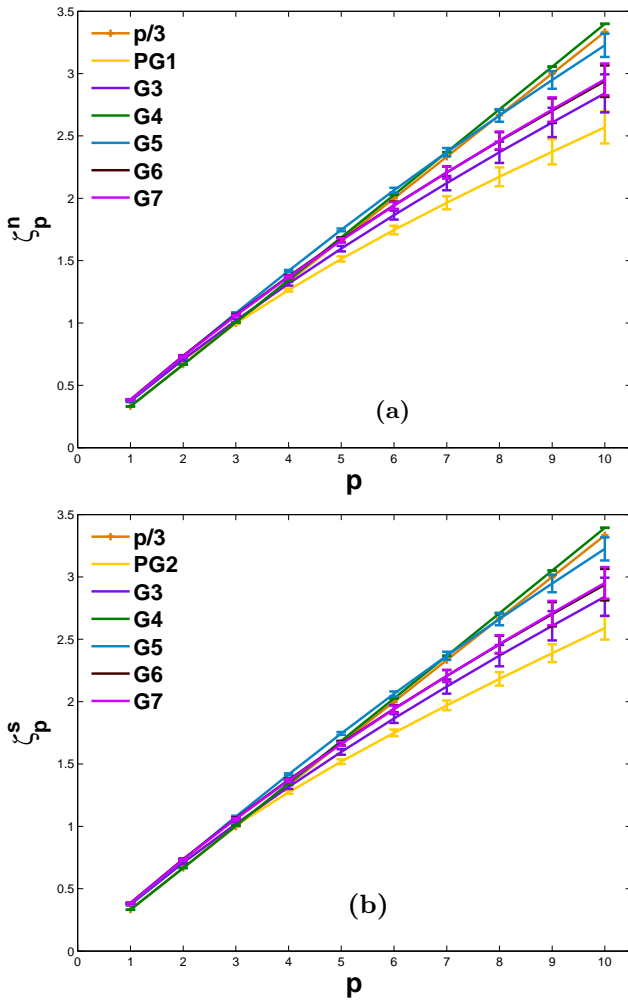


FIG. 2. Plots versus order p of the multiscaling exponents: (a) ζ_p^n and (b) ζ_p^s , for the shell-model runs G3 (purple curve), G4 (green curve), G5 (sky-blue curve), G6 (brown curve), and G7 (magenta curve). PG1, PG2 are the classical-fluid-turbulence runs (yellow curve) and $\zeta^{K41} = p/3$ is denoted by the orange line.

is the K41 prediction $\zeta_p^{K41} = p/3$ and the yellow line shows the multiscaling exponents ζ_p^c of classical (superscript c), 3D-fluid turbulence. The multiscaling exponents ζ_p^i , $i \in (n, s)$, which we determine from the 3D-HVBK shell-model, show deviations from ζ_p^c ; these deviations depend on the values of ρ_n/ρ and \bar{B} . Moreover, for the run G4 ($\rho_n/\rho = 0.4$, $B = 0.9838$), the ζ_p^i 's (green lines in Figs. 2 (a) and (b)) are close to $\zeta_p^{K41} = p/3$. For the run G3 ($\rho_n/\rho = 0.25$, $B = 1.08$), the ζ_p^i 's (purple lines in Figs. 2 (a) and (b)) lie roughly between ζ_p^{K41} and ζ_p^c ; for the runs G5-G7, the differences between ζ_p^i and ζ_p^{K41} and ζ_p^c depend on p .

To understand the dependence of the multiscaling exponents ζ_p^i , $i \in (n, s)$, on ρ_n/ρ (which includes the variation of \bar{B} with temperature), we plot, in Fig. 3, ζ_p^n , for $p = 1$ to 6, versus ρ_n/ρ from our runs G1-G9. Figure 3

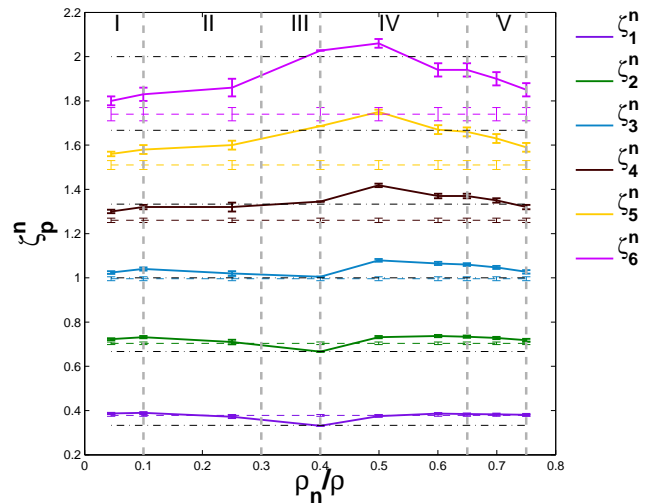


FIG. 3. Plots of ζ_p^n , for $p = 1$ to 6, versus ρ_n/ρ , from our shell-model runs G1-G9. For the purpose of reference, we show the value of a classical-fluid-turbulence exponent ζ_p^c , for order p , by a horizontal, dashed line; different colors indicate different values of the order p . The black, dot-dashed lines indicates $\zeta_p^{K41} = p/3$.

shows that, depending on the values of ρ_n/ρ , the behavior of the exponents ζ_p^n can be classified *roughly* into five regions I-V (demarcated by grey, dashed, vertical lines on the plot). Region I ($\rho_n/\rho \lesssim 0.1$): The values of ζ_p^n are close to the classical-fluid-turbulence exponents ζ_p^c . Region II ($0.1 < \rho_n/\rho < 0.3$): $\zeta_p^n > \zeta_p^c$, for $p \geq 3$ and, for $p = 1, 2$, $\zeta_p^n \simeq \zeta_p^c$. Region III ($0.3 \lesssim \rho_n/\rho \lesssim 0.4$): $\zeta_p^n \simeq \zeta_p^{K41}$. Region IV ($0.4 < \rho_n/\rho \lesssim 0.65$): ζ_p^n show significant deviations from both ζ_p^c and ζ_p^{K41} . Region V ($\rho_n/\rho > 0.65$): ζ_p^n show a tendency to move towards ζ_p^c .

We now examine the dependence of the multiscaling exponents ζ_p^i , $i \in (n, s)$ on ρ_n/ρ , while keeping the coefficient of mutual friction $B = 1.5$ fixed, in runs B1-B19. These runs allow us to classify the behavior of ζ_p^i , $i \in (n, s)$, as a function of ρ_n/ρ , more clearly than the runs G1-G9. In the Supplemental Material, in Table IV we list the values of ζ_p^i , $i \in (n, s)$, which we extract from Σ_p^i (Eq. 20), for $p = 1$ to 6, $i \in (n, s)$; each row of this Table has two lines; the first and second lines contain the values of ζ_p^n and ζ_p^s , respectively. For these runs $\zeta_p^n \simeq \zeta_p^s$. In Fig. 4 we plot ζ_p^n , versus ρ_n/ρ , for $p = 1$ to 6 in runs B1-B19. These plots show two regions ($0.1 < \rho_n/\rho < 0.3$ and $0.4 < \rho_n/\rho < 0.65$) with clear bumps, where the values of ζ_p^n deviate significantly from both $\zeta_p^{K41} (< \zeta_p^n)$ and $\zeta_p^c (< \zeta_p^n)$. We classify *roughly* the behaviors of these ζ_p^n into six regions I-VI (demarcated by grey, dashed, vertical lines in Fig. 4), which we describe below. Region I ($\rho_n/\rho \lesssim 0.1$): $\zeta_p^n \simeq \zeta_p^c$. Region II ($0.1 < \rho_n/\rho < 0.3$): ζ_p^n differs significantly from both ζ_p^c and ζ_p^{K41} , with $\zeta_p^c < \zeta_p^n$ and $\zeta_p^{K41} < \zeta_p^n$. Region III ($0.3 \lesssim \rho_n/\rho \lesssim 0.4$): $\zeta_p^n \simeq \zeta_p^{K41}$. Region IV ($0.4 < \rho_n/\rho < 0.65$): ζ_p^n differs significantly from both

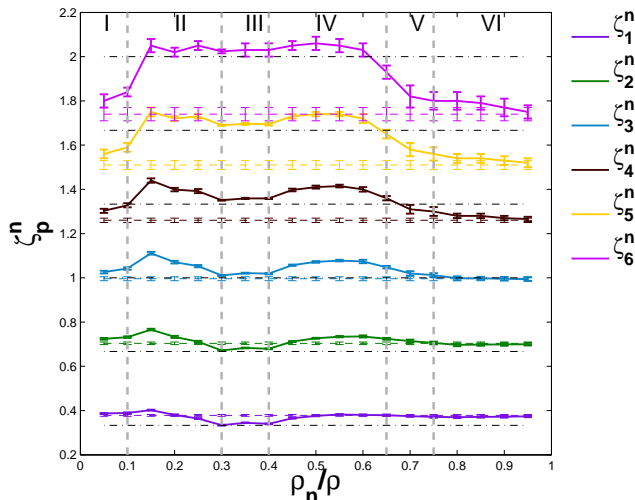


FIG. 4. Plots of ζ_p^n , for $p = 1$ to 6 , versus ρ_n/ρ , from our shell-model runs B1-B19. For the purpose of reference, we show the value of a classical-fluid-turbulence exponent ζ_p^c , for order p , by a horizontal, dashed line; different colors indicate different values of the order p . The black, dot-dashed lines indicates $\zeta_p^{K41} = p/3$. In the shell-model runs B1-B19, we keep the mutual-friction coefficient $B = 1.5$ fixed.

ζ_p^c and ζ_p^{K41} , with $\zeta_p^c < \zeta_p^n$ and $\zeta_p^{K41} < \zeta_p^n$. Region V ($0.65 \gtrsim \rho_n/\rho < 0.75$): ζ_p^n shows a tendency to move towards ζ_p^c . Region VI ($\rho_n/\rho \gtrsim 0.75$): $\zeta_p^n \simeq \zeta_p^c$.

We also explore the dependence of the multiscaling exponents ζ_p^i , $i \in (n, s)$, on the mutual-friction coefficient B , while keeping the normal-fluid-density fraction $\rho_n/\rho = 0.5$ fixed. In our 3D-HVBK-shell-model runs R1-R12, we systematically vary the values of B ; we list the values of ζ_p^i , $i \in (n, s)$ obtained from Σ_p^i (Eq. 20), for $p = 1$ to 6 , in Table V in the Supplemental Material; each row of this Table has two lines; the first and second lines contain, respectively, the values of ζ_p^n and ζ_p^s . In Fig. 5 we plot ζ_p^n versus B , for $p = 1$ to 6 , for the runs R1-R12; the exponents ζ_p^n deviate significantly from their classical-fluid-turbulence counterparts ζ_p^c , in the range $1 \leq B \leq 3$, with $\zeta_p^n > \zeta_p^c$, for $p \geq 3$, $\zeta_1^n < \zeta_1^c$, and ζ_2^n marginally larger than ζ_2^c . As $B \rightarrow 0.1$ (small values) and $B \rightarrow 10$ (large values) the multiscaling exponents $\zeta_p^n \simeq \zeta_p^c$, because, in the limit $B \rightarrow 0$, the normal fluid and superfluid are uncoupled; and for very large values of B , the coupling is so strong that single-fluid-turbulence results emerge.

We have checked explicitly that all the values of ζ_p^n and ζ_p^s , which we have reported above, satisfy the convexity inequality Eq. (21). We illustrate this in the plots of Fig. 6.

IV. CONCLUSIONS

We have carried out extensive numerical simulations of the 3D-HVBK shell-model, specifically to study the

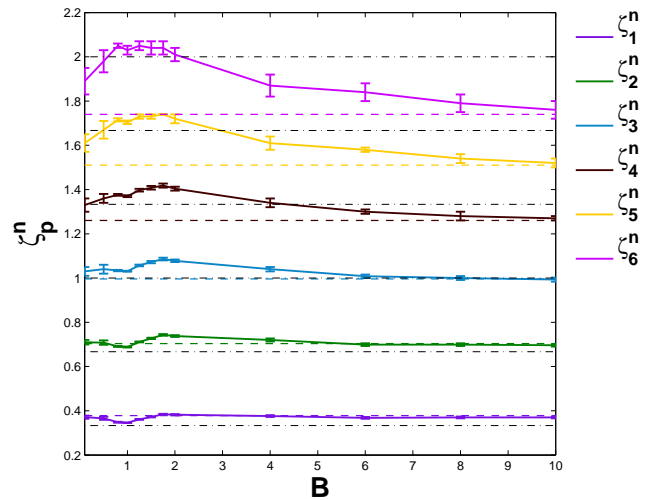


FIG. 5. Plot of ζ_p^n , for $p = 1$ to 6 , versus ρ_n/ρ , from the shell-model runs R1-R12. For the purpose of reference, we show the value of a classical-fluid-turbulence exponent ζ_p^c , for order p , by a horizontal, dashed line; different colors indicate different values of the order p . The black, dot-dashed lines indicates $\zeta_p^{K41} = p/3$. In the shell-model runs R1-R12, we keep the normal-fluid density fraction $\rho_n/\rho = 0.5$ fixed.

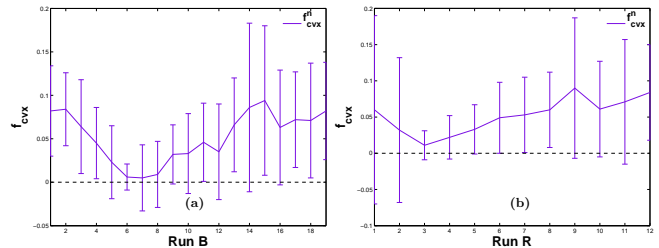


FIG. 6. Plots of (a) f_{cvx}^n for the runs B1-B19 ($B = 1.5$); (b) f_{cvx}^n for the runs R1-R12 ($\rho_n/\rho = 0.5$), where $f_{cvx}^i = (p_3 - p_1)\zeta_{2p_2}^i - (p_3 - p_2)\zeta_{2p_1}^i - (p_2 - p_1)\zeta_{2p_3}^i$, $i \in (n, s)$, and we take $p_1 = 1$, $p_2 = 2$, and $p_3 = 3$. The multiscaling exponents ζ_p^i , $i \in (n, s)$, satisfy the convexity constraint, if $f_{cvx}^i > 0$, for any three positive integers $p_1 \leq p_2 \leq p_3$. The x -axis label in the above plots indicates the run index, e.g., B1.

multiscaling of structure functions in superfluid turbulence, because such multiscaling has been studied much less than its counterpart in classical-fluid turbulence. Experimental investigations of turbulence in liquid helium, below the superfluid transition temperature T_λ , have provided evidence for multiscaling, in the inertial range [61–63]. These experiments have also motivated our study. Direct numerical simulations of models for superfluids, e.g., the Gross-Pitaevskii equation and the HVBK two-fluid equations, have not been able to cover the large range of length scales that are required to obtain reliable data for high-order structure functions. Shell models, based on the HVBK two-fluid equations, have been used to study the statistical properties of 3D superfluid turbulence in both ^4He [24, 26] and $^3\text{He-B}$ [24, 25]; these

studies have elucidated the natures of energy spectra and fluxes, for both forced, statistically steady and decaying superfluid turbulence. The only detailed investigation of the multiscaling behavior of structure functions is an HVBK-shell-model study [26]. This study has shown that, for $\rho_n/\rho \leq 0.1$ and $\rho_n/\rho \leq 0.9$, the multiscaling exponents are close to those in classical-fluid turbulence; whereas, in the range $0.25 \leq \rho_n/\rho \leq 0.5$, high-order multiscaling exponents deviate significantly from, and are smaller than, their classical-fluid-turbulence counterparts.

Our extensive study of the 3D-HVBK shell model has shown that the multiscaling of structure functions in superfluid turbulence is more complex than that reported in Ref. [26]. However, our results agree with those of Ref. [26] in that, for $\rho_n/\rho \lesssim 0.1$ and $\rho_n/\rho \gtrsim 0.75$, the multiscaling exponents are close to the classical-fluid-turbulence values. Moreover, we find that there are two regions, with $0.1 < \rho_n/\rho < 0.3$ and $0.4 < \rho_n/\rho < 0.65$, where the multiscaling exponents are larger than their classical-fluid-turbulence and K41 counterparts, i.e., $\zeta_p^i > \zeta_p^c$ and $\zeta_p^i > \zeta_p^{K41}$, $i \in (n, s)$. In the

range $0.3 \lesssim \rho_n/\rho \lesssim 0.4$, these exponents are close to the K41 prediction, i.e., $\zeta_p^i \simeq \zeta_p^{K41}$. We have also investigated the dependence of the multiscaling exponents on the mutual-friction coefficient B , with $\rho_n/\rho = 0.5$ fixed; our results show that, for small (weak-coupling limit) and large (strong-coupling limit) values of B , the multiscaling exponents tend to their classical-fluid-turbulence values, whereas, in the range $1 \lesssim B \lesssim 3$, there are deviations from the classical-fluid-turbulence behavior $\zeta_p^i > \zeta_p^c$, for $p \geq 3$. We hope our extensive study of the multiscaling of structure functions in the 3D-HVBK shell-model will stimulate detailed experimental and DNS studies of such multiscaling in quantum-fluid turbulence in different quantum fluids.

ACKNOWLEDGMENTS

We thank CSIR, UGC, DST (India) and the Indo-French Centre for Applied Mathematics (IFCAM) for financial support, and SERC (IISc) for computational resources. VS acknowledges support from Centre Franco-Indien pour la Promotion de la Recherche Avancée (CE-FIPRA) project no. 4904. We are grateful to A. Basu and S.S. Ray for useful discussions.

-
- [1] U. Frisch, *Turbulence*, Vol. 1 (Cambridge University Press, Cambridge, UK, 1996).
- [2] C. Meneveau and K. R. Sreenivasan, *J. Fluid Mech.* **224**, 429 (1991).
- [3] K. R. Sreenivasan and R. A. Antonia, *Annu. Rev. Fluid Mech.* **29**, 435 (1997).
- [4] G. Boffetta, A. Mazzino, and A. Vulpiani, *J. Phys. A: Mathematical and Theoretical* **41**, 363001 (2008).
- [5] T. Ishihara, T. Gotoh, and Y. Kaneda, *Annu. Rev. Fluid Mech.* **41**, 165 (2009).
- [6] A. Arnèodo, R. Benzi, J. Berg, L. Biferale, E. Bodenschatz, A. Busse, E. Calzavarini, B. Castaing, M. Cencini, L. Chevillard, R. T. Fisher, R. Grauer, H. Homann, D. Lamb, A. S. Lanotte, E. Lévêque, B. Lüthi, J. Mann, N. Mordant, W.-C. Müller, S. Ott, N. T. Ouellette, J.-F. Pinton, S. B. Pope, S. G. Roux, F. Toschi, H. Xu, and P. K. Yeung (International Collaboration for Turbulence Research), *Phys. Rev. Lett.* **100**, 254504 (2008).
- [7] D. A. Donzis, P. K. Yeung, and K. R. Sreenivasan, *Phys. Fluids* **20**, 045108 (2008).
- [8] R. Pandit, P. Perlekar, and S. Ray, *Pramana* **73**, 157 (2009).
- [9] D. Biskamp and W. C. Mueller, *Phys. Plasmas* **7**, 4889 (2000).
- [10] P. D. Mininni and A. Pouquet, *Phys. Rev. Lett.* **99**, 254502 (2007).
- [11] P. D. Mininni and A. Pouquet, *Phys. Rev. E* **80**, 025401 (2009).
- [12] G. Sahoo, P. Perlekar, and R. Pandit, *New J. Phys.* **13**, 013036 (2011).
- [13] R. J. Donnelly, *Quantized vortices in helium II*, Vol. 2 (Cambridge University Press, 1991).
- [14] M. S. Paoletti and D. P. Lathrop, *Annu. Rev. Condens. Matter Phys.* **2**, 213 (2011).
- [15] L. Skrbek and K. R. Sreenivasan, *Phys. Fluids* **24**, 011301 (2012).
- [16] N. G. Berloff, M. Brachet, and N. P. Proukakis, *Proc. Natl. Acad. Sci. USA* **111**, 4675 (2014).
- [17] V. Shukla, A. Gupta, and R. Pandit, arXiv preprint arXiv:1409.4537 (2014).
- [18] A. N. Kolmogorov, *Dokl. Akad. Nauk SSSR* **30**, 301 (1941).
- [19] A. N. Kolmogorov, *Dokl. Akad. Nauk SSSR* **31**, 538 (1941).
- [20] A. N. Kolmogorov, *Dokl. Akad. Nauk SSSR* **32**, 16 (1941).
- [21] V. Shukla, M. Brachet, and R. Pandit, *New J. Phys.* **15**, 113025 (2013).
- [22] V. Shukla, M. Brachet, and R. Pandit, arXiv preprint arXiv:1412.0706 (2014).
- [23] V. Shukla, *Particles and Fields in Superfluid Turbulence: Numerical and Theoretical Studies*, Ph.D. thesis, Indian Institute of Science, Bangalore (2014), unpublished.
- [24] D. H. Wacks and C. F. Barenghi, *Phys. Rev. B* **84**, 184505 (2011).
- [25] L. Boué, V. L'vov, A. Pomyalov, and I. Procaccia, *Phys. Rev. B* **85**, 104502 (2012).
- [26] L. Boué, V. L'vov, A. Pomyalov, and I. Procaccia, *Phys. Rev. Lett.* **110**, 014502 (2013).
- [27] A. M. Obukhov, *Atmos. Oceanic Phys.* **10**, 127 (1974).
- [28] V. N. Desnyansky and E. A. Novikov, *Prikl. Mat. Mekh.* **38**, 507 (1974).
- [29] E. B. Gledzer, *Sov. Phys. Dokl. SSSR* **18**, 216 (1973).
- [30] K. Ohkitani and M. Yamada, *Prog. Theor. Phys.* **81**, 32941 (1982).
- [31] M. H. Jensen, G. Paladin, and A. Vulpiani, *Phys. Rev. A* **43**, 798 (1991).

- [32] D. Pisarenko, L. Biferale, D. Courvoisier, U. Frisch, and M. Vergassola, *Phys. Fluids A* **5**, 2533 (1993).
- [33] S. Dhar, A. Sain, A. Pande, and R. Pandit, *Pramana J. Phys.: Special Issue on Nonlinearity and Chaos in the Physical Sciences* **48**, 325 (1997).
- [34] S. K. Dhar, A. Sain, and R. Pandit, *Phys. Rev. Lett.* **78**, 2964 (1997).
- [35] L. Biferale, *Annu. Rev. Fluid Mech.* **35**, 441 (2003).
- [36] T. Bohr, M. H. Jensen, G. Paladin, and A. Vulpiani, *Dynamical systems approach to turbulence*, Cambridge Nonlinear Science Series (Cambridge University Press, UK, 2005).
- [37] P. D. Ditlevsen, *Turbulence and shell models* (Cambridge University Press, UK, 2010).
- [38] V. S. L'vov, E. Podivilov, A. Pomyalov, I. Procaccia, and D. Vandembroucq, *Phys. Rev. E* **58**, 1811 (1998).
- [39] A. Basu, A. Sain, S. K. Dhar, and R. Pandit, *Phys. Rev. Lett.* **81**, 2687 (1998).
- [40] C. Kalelkar and R. Pandit, *Phys. Rev. E* **69**, 046304 (2004).
- [41] G. Sahoo, D. Mitra, and R. Pandit, *Phys. Rev. E* **81**, 036317 (2010).
- [42] P. Frick and D. Sokoloff, *Phys. Rev. E* **57**, 4155 (1998).
- [43] A. Brandenburg, K. Enqvist, and P. Olesen, *Phys. Rev. D* **54**, 1291 (1996).
- [44] P. Giuliani and V. Carbone, *Europhys. Lett.* **43**, 527 (1998).
- [45] D. Hori, M. Furukawa, S. Ohsaki, and Z. Yoshida, *J. Plasma Fusion Res.* **81**, 141 (2005).
- [46] D. Hori and H. Miura, *J. Plasma Fusion Res.* **3**, S1053 (2008).
- [47] S. Galtier, *Phys. Rev. E* **77**, 015302 (2008).
- [48] D. Banerjee, S. S. Ray, G. Sahoo, and R. Pandit, *Phys. Rev. Lett.* **111**, 174501 (2013).
- [49] C. Kalelkar, R. Govindarajan, and R. Pandit, *Phys. Rev. E* **72**, 017301 (2005).
- [50] E. Aurell, G. Boffetta, A. Crisanti, P. Frick, G. Paladin, and A. Vulpiani, *Phys. Rev. E* **50**, 4705 (1994).
- [51] P. Giuliani, M. H. Jensen, and V. Yakhot, *Phys. Rev. E* **65**, 036305 (2002).
- [52] S. S. Ray and A. Basu, *Phys. Rev. E* **84**, 036316 (2011).
- [53] Y. Hattori, R. Rubinstein, and A. Ishizawa, *Phys. Rev. E* **70**, 046311 (2004).
- [54] D. Mitra and R. Pandit, *Phys. Rev. Lett.* **93**, 024501 (2004).
- [55] D. Mitra, S. S. Ray, and R. Pandit, *Eur. Phys. J. B* **64**, 463 (2008).
- [56] S. S. Ray, D. Mitra, and R. Pandit, *New J. Phys.* **10**, 033003 (2008).
- [57] P. E. Roche, C. F. Barenghi, and E. Lévêque, *Europhys. Lett.* **87**, 54006 (2009).
- [58] C. J. Gorter and J. H. Mellink, *Physica* **15**, 285 (1949).
- [59] S. M. Cox and P. C. Matthews, *J. Comput. Phys.* **176**, 430 (2002).
- [60] R. J. Donnelly and C. F. Barenghi, *J. Phys. Chem. Ref. Data* **27**, 1217 (1998).
- [61] J. Maurer and P. Tabeling, *Europhys. Lett.* **43**, 29 (1998).
- [62] J. Salort, B. Chabaud, E. Lévêque, and P.-E. Roche, in *J. Phys. Conf. Ser.*, Vol. 318 (IOP Publishing, 2011) p. 042014.
- [63] J. Salort, B. Chabaud, E. Lévêque, and P.-E. Roche, *Europhys. Lett.* **97**, 34006 (2012).

SUPPLEMENTAL MATERIAL

	ρ_n/ρ	ζ_1^n	ζ_2^n	ζ_3^n	ζ_4^n	ζ_5^n	ζ_6^n
	(B)	ζ_1^s	ζ_2^s	ζ_3^s	ζ_4^s	ζ_5^s	ζ_6^s
PG1	–	0.378 ± 0.004	0.704 ± 0.006	0.996 ± 0.009	1.26 ± 0.01	1.51 ± 0.02	1.74 ± 0.03
PG2	–	0.383 ± 0.003	0.714 ± 0.005	1.007 ± 0.007	1.27 ± 0.01	1.52 ± 0.02	1.75 ± 0.02
G1a	0.0450	0.378 ± 0.008	0.70 ± 0.01	0.99 ± 0.02	1.26 ± 0.03	1.50 ± 0.05	1.73 ± 0.07
	(1.5260)	0.378 ± 0.008	0.70 ± 0.01	0.99 ± 0.02	1.26 ± 0.03	1.50 ± 0.05	1.73 ± 0.07
G1	0.0450	0.387 ± 0.003	0.723 ± 0.004	1.024 ± 0.006	1.300 ± 0.008	1.56 ± 0.01	1.80 ± 0.02
	(1.5260)	0.384 ± 0.003	0.721 ± 0.004	1.022 ± 0.006	1.300 ± 0.008	1.55 ± 0.01	1.80 ± 0.02
G2	0.0998	0.390 ± 0.003	0.732 ± 0.005	1.040 ± 0.007	1.32 ± 0.01	1.58 ± 0.02	1.83 ± 0.03
	(1.3255)	0.389 ± 0.003	0.731 ± 0.005	1.040 ± 0.007	1.32 ± 0.01	1.58 ± 0.02	1.83 ± 0.03
G3	0.2503	0.372 ± 0.006	0.71 ± 0.01	1.02 ± 0.01	1.32 ± 0.02	1.60 ± 0.02	1.86 ± 0.04
	(1.0765)	0.372 ± 0.006	0.71 ± 0.01	1.02 ± 0.01	1.32 ± 0.02	1.60 ± 0.02	1.86 ± 0.04
G4	0.4004	0.3309 ± 0.0001	0.6663 ± 0.0001	1.0046 ± 0.0001	1.3446 ± 0.0001	1.6858 ± 0.0002	2.0276 ± 0.0003
	(0.9838)	0.3310 ± 0.0001	0.6664 ± 0.0001	1.0044 ± 0.0001	1.3441 ± 0.0001	1.6847 ± 0.0002	2.0259 ± 0.0002
G5	0.4994	0.375 ± 0.004	0.732 ± 0.005	1.079 ± 0.006	1.418 ± 0.008	1.75 ± 0.01	2.06 ± 0.02
	(0.9848)	0.374 ± 0.003	0.732 ± 0.005	1.079 ± 0.006	1.417 ± 0.008	1.74 ± 0.01	2.06 ± 0.02
G6	0.6003	0.386 ± 0.003	0.737 ± 0.005	1.065 ± 0.007	1.37 ± 0.01	1.67 ± 0.02	1.94 ± 0.03
	(1.0447)	0.385 ± 0.003	0.737 ± 0.005	1.064 ± 0.007	1.37 ± 0.01	1.66 ± 0.02	1.94 ± 0.03
G7	0.6493	0.384 ± 0.003	0.734 ± 0.005	1.060 ± 0.006	1.37 ± 0.01	1.66 ± 0.02	1.94 ± 0.03
	(1.1034)	0.384 ± 0.003	0.734 ± 0.004	1.060 ± 0.006	1.37 ± 0.01	1.66 ± 0.02	1.94 ± 0.03
G8	0.6995	0.383 ± 0.003	0.728 ± 0.004	1.047 ± 0.007	1.35 ± 0.01	1.63 ± 0.02	1.90 ± 0.03
	(1.1924)	0.383 ± 0.003	0.728 ± 0.004	1.046 ± 0.007	1.35 ± 0.01	1.63 ± 0.02	1.90 ± 0.03
G9	0.7501	0.381 ± 0.004	0.718 ± 0.006	1.027 ± 0.008	1.32 ± 0.01	1.59 ± 0.02	1.85 ± 0.03
	(1.3267)	0.380 ± 0.004	0.718 ± 0.006	1.027 ± 0.008	1.32 ± 0.01	1.59 ± 0.02	1.85 ± 0.03

TABLE III. Multiscaling exponents ζ_p from our shell-model runs PG1, PG2, and G1 – G9; each row of the Table has two lines; the first and second lines contain, respectively, the values of ζ_p^n and ζ_p^s . In the second column, ρ_n/ρ is the normal-fluid density fraction (first line) and B is the mutual-friction coefficient (second line, in parentheses).

	ρ_n/ρ	ζ_1	ζ_2	ζ_3	ζ_4	ζ_5	ζ_6
B1	0.05	0.387 ± 0.002	0.724 ± 0.004	1.026 ± 0.006	1.303 ± 0.009	1.56 ± 0.02	1.80 ± 0.03
		0.384 ± 0.002	0.720 ± 0.004	1.023 ± 0.006	1.301 ± 0.009	1.56 ± 0.02	1.80 ± 0.03
B2	0.10	0.389 ± 0.003	0.732 ± 0.004	1.042 ± 0.006	1.328 ± 0.009	1.59 ± 0.02	1.84 ± 0.02
		0.388 ± 0.003	0.733 ± 0.004	1.045 ± 0.005	1.333 ± 0.008	1.60 ± 0.01	1.85 ± 0.02
B3	0.15	0.402 ± 0.002	0.766 ± 0.004	1.111 ± 0.006	1.44 ± 0.01	1.75 ± 0.02	2.05 ± 0.03
		0.395 ± 0.002	0.761 ± 0.004	1.107 ± 0.006	1.44 ± 0.01	1.75 ± 0.02	2.05 ± 0.03
B4	0.20	0.380 ± 0.003	0.733 ± 0.005	1.071 ± 0.006	1.399 ± 0.008	1.72 ± 0.01	2.02 ± 0.02
		0.376 ± 0.003	0.730 ± 0.005	1.069 ± 0.006	1.397 ± 0.008	1.71 ± 0.01	2.02 ± 0.02
B5	0.025	0.364 ± 0.002	0.711 ± 0.004	1.053 ± 0.005	1.392 ± 0.009	1.73 ± 0.01	2.05 ± 0.02
		0.360 ± 0.002	0.708 ± 0.004	1.051 ± 0.005	1.390 ± 0.007	1.72 ± 0.01	2.05 ± 0.02
B6	0.30	0.334 ± 0.002	0.672 ± 0.002	1.011 ± 0.002	1.351 ± 0.002	1.690 ± 0.003	2.024 ± 0.009
		0.334 ± 0.002	0.671 ± 0.002	1.010 ± 0.002	1.350 ± 0.002	1.688 ± 0.003	2.01 ± 0.009
B7	0.35	0.345 ± 0.001	0.683 ± 0.002	1.021 ± 0.002	1.359 ± 0.003	1.696 ± 0.005	2.03 ± 0.01
		0.3385 ± 0.0009	0.677 ± 0.001	1.015 ± 0.002	1.355 ± 0.003	1.693 ± 0.005	2.02 ± 0.01
B8	0.40	0.340 ± 0.002	0.679 ± 0.002	1.019 ± 0.003	1.359 ± 0.003	1.695 ± 0.006	2.03 ± 0.01
		0.339 ± 0.001	0.680 ± 0.002	1.021 ± 0.002	1.361 ± 0.002	1.699 ± 0.006	2.03 ± 0.01
B9	0.45	0.365 ± 0.002	0.712 ± 0.002	1.057 ± 0.003	1.397 ± 0.006	1.73 ± 0.01	2.05 ± 0.02
		0.353 ± 0.001	0.699 ± 0.002	1.046 ± 0.003	1.389 ± 0.005	1.72 ± 0.01	2.05 ± 0.03
B10	0.50	0.376 ± 0.002	0.727 ± 0.002	1.072 ± 0.004	1.410 ± 0.007	1.74 ± 0.01	2.06 ± 0.03
		0.365 ± 0.002	0.720 ± 0.002	1.068 ± 0.004	1.408 ± 0.007	1.74 ± 0.01	2.05 ± 0.03
B11	0.55	0.382 ± 0.002	0.734 ± 0.003	1.078 ± 0.004	1.415 ± 0.006	1.74 ± 0.01	2.05 ± 0.03
		0.370 ± 0.002	0.727 ± 0.003	1.075 ± 0.004	1.414 ± 0.007	1.74 ± 0.01	2.06 ± 0.03
B12	0.60	0.380 ± 0.003	0.735 ± 0.005	1.074 ± 0.008	1.40 ± 0.01	1.72 ± 0.02	2.03 ± 0.03
		0.379 ± 0.003	0.734 ± 0.005	1.073 ± 0.008	1.40 ± 0.01	1.72 ± 0.02	2.03 ± 0.03
B13	0.65	0.379 ± 0.003	0.724 ± 0.004	1.048 ± 0.006	1.36 ± 0.01	1.65 ± 0.02	1.93 ± 0.03
		0.378 ± 0.003	0.723 ± 0.004	1.047 ± 0.006	1.36 ± 0.01	1.65 ± 0.02	1.93 ± 0.03
B14	0.70	0.375 ± 0.004	0.714 ± 0.007	1.02 ± 0.01	1.31 ± 0.02	1.58 ± 0.03	1.82 ± 0.05
		0.375 ± 0.005	0.714 ± 0.007	1.02 ± 0.01	1.31 ± 0.02	1.58 ± 0.03	1.82 ± 0.05
B15	0.75	0.371 ± 0.004	0.706 ± 0.006	1.012 ± 0.009	1.30 ± 0.02	1.56 ± 0.03	1.80 ± 0.04
		0.371 ± 0.004	0.705 ± 0.006	1.012 ± 0.009	1.30 ± 0.02	1.56 ± 0.03	1.80 ± 0.04
B16	0.80	0.370 ± 0.004	0.697 ± 0.006	0.998 ± 0.009	1.28 ± 0.01	1.54 ± 0.02	1.80 ± 0.04
		0.369 ± 0.004	0.697 ± 0.006	0.998 ± 0.009	1.28 ± 0.01	1.54 ± 0.02	1.80 ± 0.04
B17	0.85	0.371 ± 0.003	0.698 ± 0.005	0.998 ± 0.007	1.28 ± 0.01	1.54 ± 0.02	1.79 ± 0.03
		0.371 ± 0.003	0.698 ± 0.005	0.998 ± 0.007	1.28 ± 0.01	1.54 ± 0.02	1.79 ± 0.03
B18	0.90	0.372 ± 0.004	0.699 ± 0.006	0.996 ± 0.008	1.27 ± 0.01	1.53 ± 0.02	1.77 ± 0.04
		0.372 ± 0.004	0.698 ± 0.006	0.996 ± 0.008	1.27 ± 0.01	1.53 ± 0.02	1.77 ± 0.04
B19	0.95	0.374 ± 0.004	0.700 ± 0.006	0.994 ± 0.008	1.266 ± 0.01	1.52 ± 0.02	1.75 ± 0.03
		0.374 ± 0.004	0.699 ± 0.006	0.994 ± 0.008	1.265 ± 0.01	1.52 ± 0.02	1.75 ± 0.03

TABLE IV. Multiscaling exponents ζ_p from our shell-model runs B1-B19; each row of the Table has two lines; the first and second lines contain, respectively, the values of ζ_p^n and ζ_p^s . ρ_n/ρ is the normal-fluid density fraction; we keep the mutual-friction coefficient $B = 1.5$ fixed.

	B	ζ_1	ζ_2	ζ_3	ζ_4	ζ_5	ζ_6
R1	0.10	0.371 ± 0.007	0.71 ± 0.01	1.03 ± 0.02	1.33 ± 0.03	1.61 ± 0.04	1.89 ± 0.06
		0.370 ± 0.007	0.71 ± 0.01	1.03 ± 0.02	1.33 ± 0.03	1.61 ± 0.04	1.89 ± 0.06
R2	0.50	0.366 ± 0.007	0.708 ± 0.01	1.04 ± 0.02	1.36 ± 0.02	1.67 ± 0.04	1.98 ± 0.05
		0.366 ± 0.007	0.708 ± 0.01	1.04 ± 0.02	1.36 ± 0.02	1.67 ± 0.04	1.98 ± 0.05
R3	0.80	0.348 ± 0.002	0.691 ± 0.002	1.034 ± 0.003	1.376 ± 0.004	1.715 ± 0.007	2.05 ± 0.01
		0.347 ± 0.002	0.691 ± 0.002	1.033 ± 0.003	1.374 ± 0.004	1.712 ± 0.007	2.04 ± 0.01
R4	1.00	0.346 ± 0.001	0.688 ± 0.002	1.031 ± 0.002	1.370 ± 0.004	1.704 ± 0.008	2.03 ± 0.02
		0.345 ± 0.001	0.688 ± 0.002	1.030 ± 0.002	1.368 ± 0.004	1.700 ± 0.008	2.02 ± 0.02
R5	1.25	0.361 ± 0.002	0.711 ± 0.002	1.057 ± 0.004	1.397 ± 0.006	1.73 ± 0.01	2.05 ± 0.02
		0.359 ± 0.002	0.710 ± 0.002	1.056 ± 0.004	1.394 ± 0.006	1.72 ± 0.01	2.04 ± 0.02
R6	1.50	0.372 ± 0.002	0.727 ± 0.003	1.072 ± 0.005	1.408 ± 0.008	1.73 ± 0.01	2.04 ± 0.03
		0.370 ± 0.002	0.725 ± 0.003	1.070 ± 0.005	1.405 ± 0.008	1.73 ± 0.01	2.04 ± 0.03
R7	1.75	0.384 ± 0.002	0.743 ± 0.004	1.086 ± 0.006	1.418 ± 0.009	1.74 ± 0.002	2.04 ± 0.03
		0.382 ± 0.002	0.742 ± 0.004	1.086 ± 0.006	1.417 ± 0.009	1.73 ± 0.002	2.04 ± 0.03
R8	2.00	0.382 ± 0.003	0.738 ± 0.004	1.078 ± 0.006	1.404 ± 0.009	1.72 ± 0.02	2.01 ± 0.03
		0.382 ± 0.003	0.738 ± 0.004	1.077 ± 0.006	1.403 ± 0.009	1.73 ± 0.02	2.01 ± 0.03
R9	4.00	0.376 ± 0.004	0.720 ± 0.007	1.04 ± 0.01	1.34 ± 0.02	1.61 ± 0.03	1.87 ± 0.05
		0.376 ± 0.004	0.720 ± 0.007	1.04 ± 0.01	1.34 ± 0.02	1.61 ± 0.03	1.87 ± 0.05
R10	6.00	0.368 ± 0.004	0.699 ± 0.006	1.008 ± 0.008	1.30 ± 0.01	1.58 ± 0.02	1.84 ± 0.04
		0.368 ± 0.004	0.699 ± 0.006	1.008 ± 0.008	1.30 ± 0.01	1.58 ± 0.02	1.84 ± 0.04
R11	8.00	0.370 ± 0.004	0.699 ± 0.006	1.000 ± 0.009	1.28 ± 0.02	1.54 ± 0.02	1.79 ± 0.04
		0.370 ± 0.004	0.699 ± 0.006	1.000 ± 0.009	1.28 ± 0.01	1.54 ± 0.02	1.79 ± 0.04
R12	10.0	0.370 ± 0.004	0.696 ± 0.006	0.993 ± 0.009	1.27 ± 0.01	1.52 ± 0.02	1.76 ± 0.04
		0.370 ± 0.004	0.696 ± 0.006	0.992 ± 0.009	1.27 ± 0.01	1.52 ± 0.02	1.76 ± 0.04

TABLE V. Multiscaling exponents ζ_p from our shell-model runs R1-R12; each row of the Table has two lines; the first and second lines contain, respectively, the values of ζ_p^n and ζ_p^s . B is the mutual-friction coefficient; we keep the normal-fluid-density fraction $\rho_n/\rho = 0.5$ fixed.